

**Contract No.:**

This manuscript has been authored by Savannah River Nuclear Solutions (SRNS), LLC under Contract No. DE-AC09-08SR22470 with the U.S. Department of Energy (DOE) Office of Environmental Management (EM).

**Disclaimer:**

The United States Government retains and the publisher, by accepting this article for publication, acknowledges that the United States Government retains a non-exclusive, paid-up, irrevocable, worldwide license to publish or reproduce the published form of this work, or allow others to do so, for United States Government purposes.

# Remotely Detected Vehicle Mass from Engine Torque-Induced Frame Twisting

Troy R. McKay<sup>a</sup>, Carl Salvaggio<sup>a</sup>, Jason W. Faulring<sup>a</sup>, Glenn D. Sweeney<sup>a</sup>

<sup>a</sup>Rochester Institute of Technology, Digital Imaging and Remote Sensing Laboratory, Chester F. Carlson Center for Imaging Science, College of Science, Rochester, New York, USA, 14623

## Abstract.

Determining the mass of a vehicle from ground-based passive sensor data is important for many traffic safety requirements. This work presents a method of calculating the mass of a vehicle using ground-based video and acoustic measurements. By assuming that no energy is lost in the conversion, the mass of a vehicle can be calculated from the rotational energy generated by the vehicle's engine and the linear acceleration of the vehicle over a period of time. The amount of rotational energy being output by the vehicle's engine can be calculated from its torque and angular velocity. This model relates remotely-observed, engine torque-induced frame twist to engine torque output using the vehicle's suspension parameters and engine geometry. The angular velocity of the engine is extracted from the acoustic emission of the engine, and the linear acceleration of the vehicle is calculated by remotely observing the position of the vehicle over time. This method combines these three dynamic signals; engine induced-frame twist, engine angular velocity, and the vehicle's linear acceleration, and three vehicle specific scalar parameters, into an expression that describes the mass of the vehicle. This method was tested on a semi-trailer truck and the results demonstrate a correlation of 97.7% between calculated and true vehicle mass.

**Keywords:** video tracking, vehicle mass, engine torque, frame twist.

\*Troy McKay, [troy@hyperspectralsolutions.com](mailto:troy@hyperspectralsolutions.com)

## 1 Introduction

Overloaded commercial vehicles increase the risk of accidents and cause deterioration of roads and bridges. When a truck is loaded in excess of their maximum permitted limit, they become less stable due to an elevated center of gravity which can over-strain the on-board stability systems, increasing the potential for rollover accidents and jack-knifing.<sup>1</sup> The braking capacity of a truck can be significantly reduced due to overloading.<sup>1</sup> Other risks associated with the operation of heavily-laden vehicles include an increased chance of a tire blowout and a higher likelihood of fire.<sup>1</sup> Overloaded vehicles also pose a danger to roads and bridges. The relationship between vehicle weight and pavement damage is exponential.<sup>2</sup> Bridges can experience increased fatigue damage due to continued exposure to these repeated loads.<sup>1</sup>

Traditionally, overloading enforcement is carried out by the random weighing of trucks at static weigh stations.<sup>3</sup> The trucks are driven onto scales and drivers of overloaded trucks are subjected to substantial fines. This method requires the presence of a manned staff of weigh station employees and it takes significant time to weigh the truck and issue the citation to the driver.<sup>1</sup> As a result, not all trucks are weighed, which leads to more drivers pushing the limits and driving overloaded. A method of measuring the mass of a vehicle using a ground-based, real-time, imaging and acoustic sensor system that would increase efficiency and allow overloaded vehicles to be identified and singled out. This would reduce the costs associated with manning a weigh station, allow appropriately-loaded vehicles to avoid unwarranted delays, and protect the public from the dangers presented by these overloaded vehicles. This paper discusses the work performed to develop a method for calculating the mass of a vehicle, remotely, using ground-based imaging and acoustic sensors.

## **2 Background**

The method described here exploits the law of conservation of energy to calculate the mass of a vehicle from its linear velocity and the rotational energy output by its engine. In order for a vehicle to accelerate, rotational energy must be transferred from the vehicle's engine to its drive wheels. During this transfer of energy, a torque is applied by the engine to the vehicle's drive shaft. An equal torque must be supplied by the vehicle's frame to prevent the engine from rotating. This torque causes the frame to twist relative to the vehicle's axles. For an engine mounted so the crankshaft is parallel to the drive shaft, known as a longitudinal engine, the frame twist would manifest as a counter-clockwise rotation (viewing the vehicle head on). An example of this engine torque-induced frame twist phenomenology can be seen in Figure 1.



(a)

(b)

Fig 1: The vehicle at rest with no engine-induced torque (1a) and the vehicle with engine-induced torque (frame twist) (1b) as the vehicle begins to accelerate from a resting state.

When the engine is applying torque to the vehicle frame,  $\tau_E$ , the frame twists relative to the axles and the vehicle's suspension springs are compressed and stretched as illustrated in Figure 2. This compression and stretching of the suspension springs causes pushing and pulling forces to be applied at the points where the frame and suspension are joined. The amount of torque generated by these forces,  $\tau_F$ , is dependent on their distance from the axis of rotation,  $r$ , and the amount of frame twist,  $\theta$ , as described by Equation 1 (the  $\theta$  and  $\theta_0$  terms accounts for the force applied non-perpendicularly to the radial axis).<sup>4</sup> The forces,  $F_1$  and  $F_2$ , are generated by the vehicle's suspension and can be described in terms of the frame twist and the total suspension spring constant,  $k_s$ , as given in Equations 2 and 3. By combining these equations, the torque generated by the suspension can be described as a function of frame twist (Equation 4). Since the torque the engine is applying to the frame is equal in magnitude and opposite in direction to the torque the suspension is applying on the frame, the engine torque can be described as a function of

the frame twist using the relationship described in Equation 5.

$$\tau_F(t) = r \cdot \cos(\theta(t) + \theta_0) \cdot (F_2 - F_1) \quad (1)$$

$$F_1(t) = -\frac{k_s \cdot r \cdot \tan(\theta(t))}{2} \quad (2)$$

$$F_2(t) = \frac{k_s \cdot r \cdot \tan(\theta(t))}{2} \quad (3)$$

$$\tau_F(t) = k_s \cdot r^2 \cdot \cos(\theta(t) + \theta_0) \cdot \tan \theta(t) \quad (4)$$

$$\tau_E(t) = -k_s \cdot r^2 \cdot \cos(\theta(t) + \theta_0) \cdot \tan \theta(t) \quad (5)$$

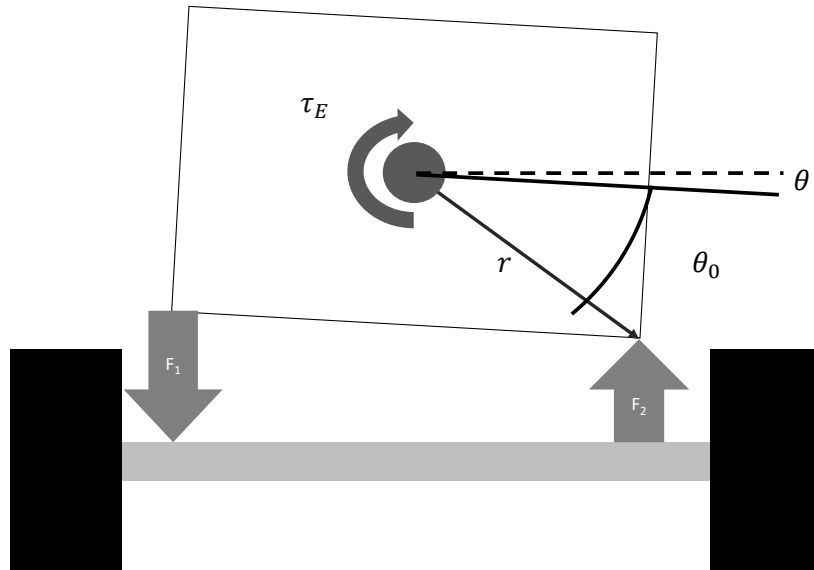


Fig 2: Longitudinal engine imparting torque,  $\tau_E$ , to the vehicle frame causing it to twist until the torque generated by the suspension forces ( $F_1$  and  $F_2$ ) are sufficient to match

Now that the torque being created by the engine has been described in terms of the amount of rotational deflection of the vehicle, the next step is to describe how much rotational power the engine is creating. Rotational power is defined by the torque and angular velocity of the rotating shaft (Equation 6).<sup>5</sup> To calculate the power output of the engine, the angular velocity of the engine,  $\omega_E(t)$ , must be measured. The angular velocity of the engine can be determined directly from the acoustic emissions of the engine. By substituting Equation 5 into Equation 6, the power output of the engine can be expressed in terms of the frame twist and the engine frequency (along with several vehicle-specific scalar constants).

$$P_E(t) = \tau_E(t) \cdot \omega_E(t) \quad (6)$$

$$P_E(t) = -\omega_E(t) \cdot k_s \cdot r^2 \cdot \cos(\theta(t) + \theta_0) \cdot \tan \theta(t) \quad (7)$$

Assuming that all of the rotational power being generated by the engine is converted into linear vehicle motion, the definite integral of the power output of the engine would be equal to the change in kinetic energy of the vehicle as shown in Equation 8. Where  $KE(t)$  is the vehicle's kinetic energy at a time  $t$ . Substituting the expression for engine power and the standard equation for kinetic energy results in Equation 9. By assuming that the vehicle is accelerating from a resting state, solving for the mass of the vehicle,  $m$ , and taking the absolute value of the definite integral, Equation 9 can be expressed in the simplified form shown in Equation 10. Note that the absolute value of the definite integral is computed because frame twist may be positive or negative

depending on the rotation direction of the engine.

$$KE(t_f) - KE(t_0) = \int_{t_0}^{t_f} P_E(t) dt \quad (8)$$

$$\frac{1}{2} \cdot m \cdot (x'(t_f)^2 - x'(t_0)^2) = -k_s \cdot r^2 \int_{t_0}^{t_f} \omega_E(t) \cdot \cos(\theta(t) + \theta_0) \cdot \tan \theta(t) dt \quad (9)$$

$$m = \frac{2 \cdot k_s \cdot r^2 \left| \int_{t_0}^{t_f} \omega_E(t) \cdot \cos(\theta(t) + \theta_0) \cdot \tan \theta(t) dt \right|}{x'(t_f)^2} \quad (10)$$

From Equation 10, the mass of the vehicle can be solved for in terms of three dynamic values; the engine's angular velocity,  $\omega_E(t)$ , frame twist,  $\theta(t)$ , the velocity of the vehicle,  $x'(t)$ , along with three vehicle-specific scalar constants; the spring constant of the suspension,  $k_s$ , the distance from the engine's axis of rotation to the suspension spring,  $r$ , and the angle of the engine force relative to the suspension spring,  $\theta_0$ . The dynamic values can be measured remotely, however, the scalar constants will need to be estimated based on vehicle type/class.

### 3 Methodology

In the previous section, a method was described to calculate the mass of a vehicle from three dynamic values and three scalar constants. This section will describe how the three dynamic values can be extracted from remotely-sensed data.

#### 3.1 Frame Twist

Video of the test vehicle was collected from a front-on view point using a conventional Canon EOS Rebel T2i DSLR camera as the vehicle accelerated from a stationary state towards the camera's

position. A normalized correlation-based video tracking algorithm was used to track and isolate the same region of the vehicle’s grill for each frame (based on the method described by Gonzalez and Woods<sup>6</sup>). The algorithm was designed to track the location of a predefined region, and to be tolerant of small frame-to-frame changes in scale and rotation. An example of the results of the tracking algorithm can be seen in Figure 3. The grill was chosen for its numerous long parallel lines, which allowed for sub-pixel measurements of the overall angular orientation to be made. Each isolated grill region extracted by the tracking algorithm was rotated using an affine transformation and bilinear resampling of digital count values. The rotated image was cropped to remove the edge artifacts caused by the rotation, and the summed standard deviation was calculated for each vertical column of pixels in the cropped region using Equation 11

$$V = \sum_{j=1}^m \sqrt{\frac{1}{n} \sum_{i=1}^n (x_{i,j} - \bar{x}_j)^2} \quad (11)$$

where  $V$  is a scalar value that quantifies the total vertical variability of the image,  $m$  is the number of columns of pixels in the image,  $n$  is the number of rows of pixels in the image,  $x_{i,j}$  is the intensity value for the pixel at location  $(i, j)$ , and  $\bar{x}_j$  is the average intensity value of the pixels in column  $j$ . This scalar value  $V$  would have a value of zero if each row of the image was identical. This was repeated for a range of rotation values bounding the expected rotation of the vehicle during its acceleration period. The rotation that resulted in the minimum scalar sum was selected as the rotation of the grill (relative to the vertical image axis). The process was repeated for each image frame as the vehicle was in motion. Figure 4 illustrates this approach for determining the vehicle’s rotation.



Fig 3: An image frame with the extracted grill region identified

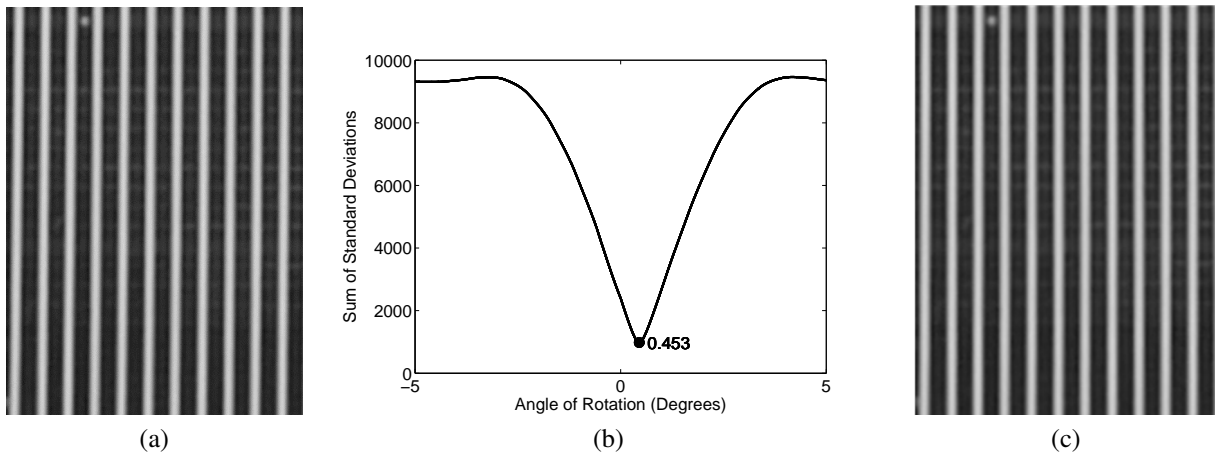


Fig 4: In order to determine the angle of rotation of the grill, the unrotated grill image (4a) is rotated through a range of image rotations from  $-5^\circ$  to  $5^\circ$ , recording the vertical variability as a function of rotation angle (4b). The minimum depicted in (4b) corresponds to the position where the grill stands perpendicular to the horizontal image axis (4c).

### 3.2 Position

Using the same video sequence exploited in the previous section, the camera-to-vehicle distance as a function of time was calculated by observing the spacing of the grill, in pixels, utilizing

Fourier analysis. After the grill images were rotated so the grill runs perpendicular to the horizontal image axis, the average of each vertical column was taken resulting in an averaged grill profile. A Hamming window was applied to the profile to reduce instances of aliasing. The magnitude of the Fourier transform was then taken and the peak frequency was identified as the frequency of the grill, the inverse of this frequency representing the period (in pixels). See Figure 5 for an example of this process.

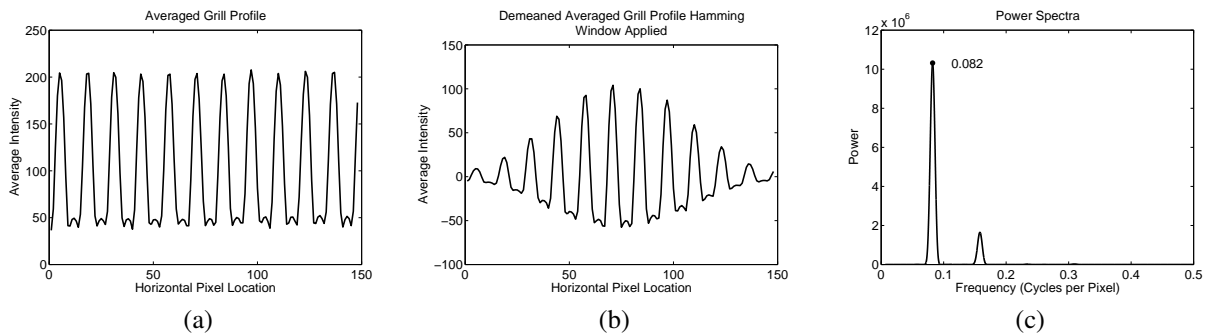


Fig 5: To calculate the grill spacing, the average grill intensity profile (5a) is demeaned and a Hamming window is applied (5b). The power spectra is then calculated and used to find the frequency of the grill (5c).

The grill spacing in pixels was calculated for each video frame using this approach. The camera-to-vehicle distance for each frame was then calculated using Equation 12, where  $d$  is the camera-to-vehicle distance,  $S$  is the grill spacing in meters,  $f$  is the focal length of the camera in meters,  $\rho$  is the pixel pitch of the camera's detector array in meters, and  $N$  is the grill spacing in pixels (the period). While the process described here required *a priori* knowledge of the grill spacing, this method could be adapted to work on any feature containing a repetitive, regularly-spaced, pattern as long as the camera-to-vehicle distance is known at one point during the collection, or

the dimensions of another feature on the vehicle is known (*e.g.* license plate).

$$d = \frac{S \cdot f}{\rho \cdot N} \quad (12)$$

### 3.3 Acoustic

Acoustic measurements of the test vehicle were collected using a microphone mounted near the path of the vehicle. The audio data was used to calculate the engine speed, again utilizing Fourier analysis. The audio data was first extracted from the video file and converted into a time-based pressure signal. A 0.3 s window of data was selected starting at time zero, a Hamming window was applied, and the magnitude of the Fourier transform was taken resulting in a power spectra. The operating frequency of the engine was calculated by locating the peaks in the power spectra associated with its 3<sup>rd</sup>, 6<sup>th</sup>, and 9<sup>th</sup> harmonic and then dividing the frequency by the harmonic number. For example, if the 3<sup>rd</sup> harmonic was found at 30 Hz, the engine frequency would be 10 Hz. Three harmonics were used because no single harmonic was found to be reliably persistent in the audio signal. The initial search locations were restricted to frequencies corresponding to the typical idling frequency of a large diesel engine, approximately 420 to 960 RPM (or 7 to 16 Hz). Once the initial engine frequency was identified, the window of data was moved forward in time by 1 ms and the process was repeated, with the search area for each harmonic being substantially restricted to within 5 Hz of the previous harmonic. If the three harmonics agreed well, the average of the three calculated engine frequency values was used. If one of the three harmonics did not agree, it was discarded. If none of the harmonics agreed well, the lowest order (3<sup>rd</sup> harmonic) was selected and used to calculate the engine frequency. This process continued until the entire pressure signal was processed, resulting in an engine frequency versus time signal. An example of

this process is shown in Figure 6.

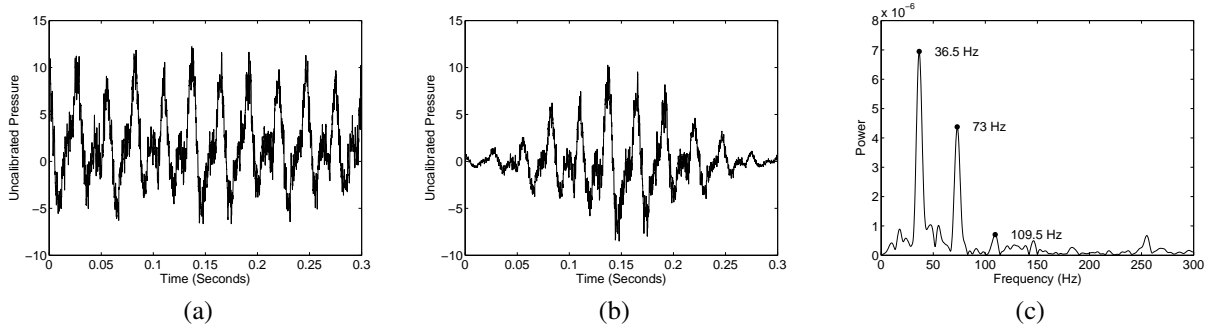


Fig 6: To calculate engine velocity, the raw acoustic signal (6a) is demeaned and a Hamming window is applied (6b). The power spectra is then calculated and used to find the 3<sup>rd</sup>, 6<sup>th</sup>, and 9<sup>th</sup> harmonic (6c).

After the acoustic data was processed into an engine frequency versus time signal, it needed to be synchronized with the data signals extracted from the video (frame twist and camera-to-vehicle distance). This synchronization was achieved through frame-by-frame analysis of on-board (truck cabin) video taken during each test run that captured the engine RPM and the vehicle speed from the vehicle's instrument panel. A still frame from this video can be seen in Figure 7. This method of synchronization was both challenging and imprecise, it is highly recommended that any future testing utilizes a synchronized data acquisition system to mitigate the need for this approach.



Fig 7: An example of the on-board video of the vehicle's instrument panel captured during each test run

#### **4 Results**

Two full-scale field tests were carried out to test the validity of the mass estimation method and the practicality of the remote sensing techniques. Each test was carried out at the Savannah River Site, a United States Department of Energy facility located in Aiken, South Carolina. Both field tests used the same tractor trailer in three load conditions; the recommended maximum load, half the recommended maximum load, and no load (empty trailer). A minimum of three test runs were completed for each load condition during both field tests. The first field test utilized a consumer-quality Canon EOS Rebel T2i DSLR camera positioned in front of the vehicle to collect video and audio as the test vehicle accelerated from a stop. The video was collected at 30 frames-per-second, and the audio was collected at 44.1 kHz. The second field test utilized a Vision Research Phantom v5.1 high-speed video camera in a similar position, and collected video at a rate of 1,200 frames-per-second. The second test utilized a PCB Piezotronics free-field condenser microphone to collect the audio data at a rate of 52 kHz.

For each test run, the video and audio data was processed using the methods described in the previous section and resulted in angular frame twist, position, and engine speed as a function of time. An example of a processed dataset from the first field test can be seen in Figure 8 and an example set from the second field test can be seen in 9. The primary difference between the processed datasets from these two independent field tests was the collection duration. The high-speed camera was only able to collect for a short time (approximately 2 seconds) due to internal memory limitations and the high frame rate. This resulted in several datasets being deemed unusable because the high-speed video was triggered too late, not capturing the initial frame twist of the vehicle. It is critical that the vehicle is measured while the frame is in a relaxed state; the frame twist at this time correlates to the zero-torque condition, and all subsequent measurements must be made relative to this initial state. For many of the data sets from the second field test, the high-speed video was initiated after the frame began to twist, but before the vehicle began moving forward (there is typically a 0.5 s to 1 s offset between when the frame first twists and the first measurable forward movement of the vehicle occurs). Due to this late initiation of the high-speed video, it was impossible to determine the amount of frame twist associated with the zero torque condition. To mitigate this, the vehicle should be observed for a considerable time, 2 s to 3 s, prior to acceleration in order to identify the zero-torque frame twist position. It should be noted, that the vehicle does not need to be completely stopped in order to identify the zero-torque condition, it must simply not be accelerating at this initial observation.

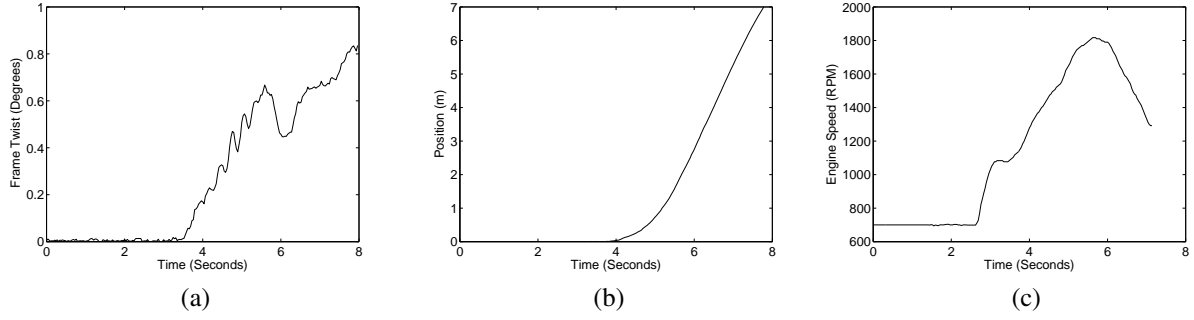


Fig 8: The angular frame twist (8a), vehicle position (8b), and engine speed (8c) of the unloaded test vehicle accelerating from a stop during the first field test

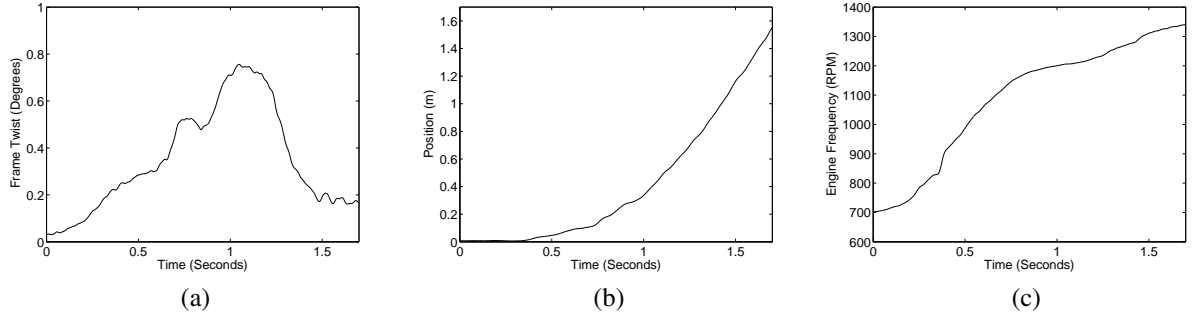


Fig 9: The angular frame twist (9a), vehicle position (9b), and engine speed (9c) of the unloaded test vehicle accelerating from a stop during the second field test

Equation 10 was modified slightly to account for the unknown spring constant,  $k_s$ , yielding Equation 13 which was used to calculate the mass-to-spring constant ratio of the test vehicle for each test run. The final time,  $t_f$ , was identified as the time where the test vehicle reached its peak velocity and the values for  $r$  and  $\theta_0$  were estimated to be 0.8 m and  $33^\circ$ , respectively. The results for the first and second field test can be seen in Figures 10 and 11, respectively.

$$\frac{m}{k_s} = \frac{2 \cdot r^2 \left| \int_{t_0}^{t_f} \omega_E(t) \cdot \cos(\theta(t) + \theta_0) \cdot \tan \theta(t) dt \right|}{x'(t_f)^2} \quad (13)$$

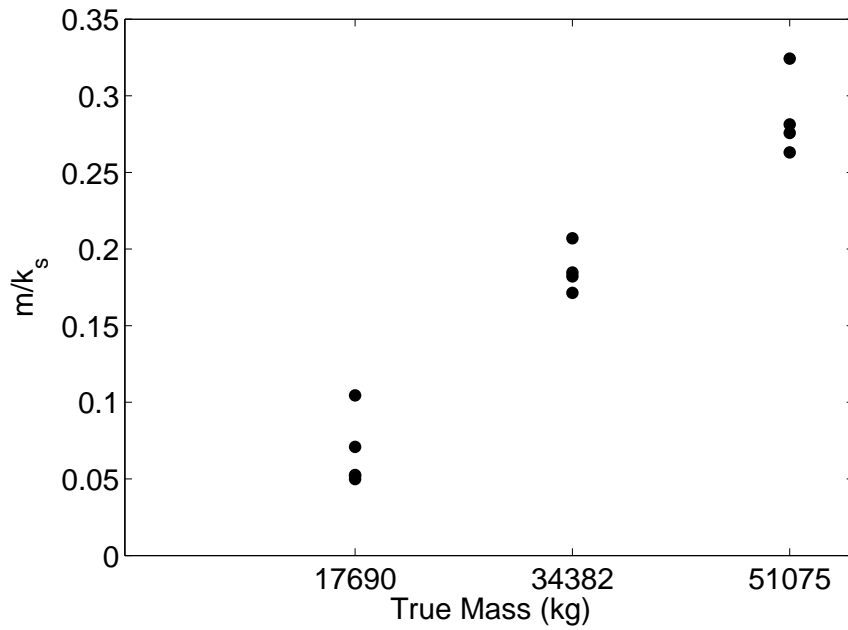


Fig 10: The calculated mass-to-spring constant ratio for each test run in the first field test versus the true test vehicle mass

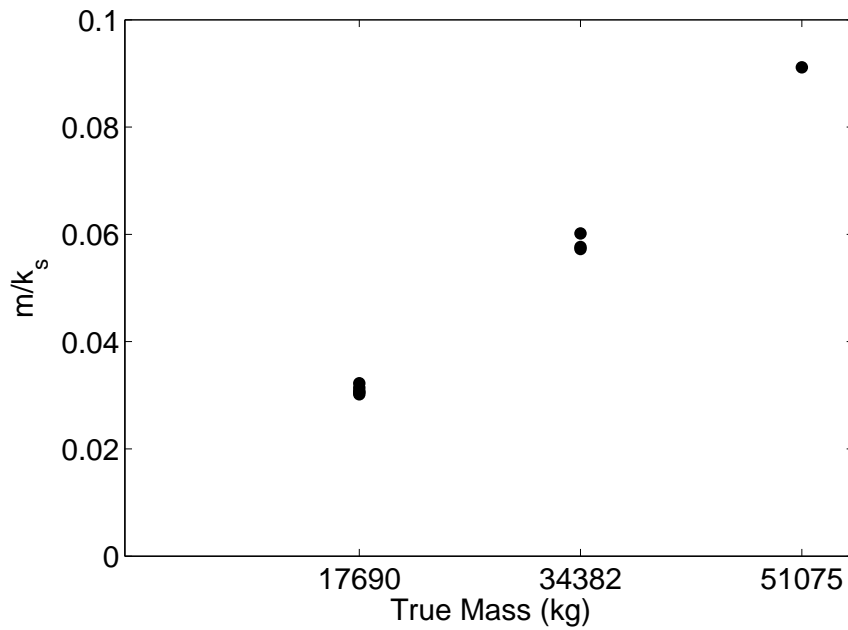


Fig 11: The calculated mass-to-spring constant ratio for each test run in the second field test versus the true test vehicle mass

## 5 Conclusions

Remotely-collected video and audio data was used to calculate a vehicle's position, engine torque-induced frame twist, and engine speed. These signals were used to calculate the vehicle's mass-to-spring constant ratio. The results depicted for the second field test (Figure 11) show a significant reduction in this mass-to-spring constant ratio when compared to the first field test (Figure 10). The reduction in this ratio was approximately a factor of three, which suggests that three times as much energy was required, during the first test as compared to the second test, to change the velocity of the test vehicle by the same amount. This discrepancy was investigated and it was determined that the data for the first field test was collected while the test vehicle was driving slightly uphill. Even a mild to moderate incline of  $3^\circ$  to  $5^\circ$  would account for the discrepancy observed between the two tests. To account for this, future testing would need to be done on roads with an incline of zero degrees, or the incline would need to be incorporated into Equation 13. The equation for the mass-to-spring constant ratio incorporating the effects of the road surface inclination angle is given here

$$\frac{m}{k_s} = \frac{r^2 \left| \int_{t_0}^{t_f} \omega_E(t) \cdot \cos(\theta(t) + \theta_0) \cdot \tan \theta(t) dt \right|}{\left( \frac{1}{2} \cdot x'(t_f)^2 \right) + (-g \cdot (h(t_f) - h(t_0)))} \quad (14)$$

where  $g$  is the force due to gravity,  $h(t_f)$  is the vehicle's elevation at time  $t_f$ , and  $h(t_0)$  is the vehicle's elevation at time  $t_0$ . This equation shows that a small change in elevation can require a significant amount of energy. For example, an increase in elevation of 5 cm would require the same amount of energy as a change in velocity of 1 m/s.

The correlation between the calculated vehicle mass-to-spring constant ratio and the true vehi-

cle mass was found to be very good for both field tests. The correlation coefficient was calculated to be 97.7% for the first test and 99.7% for the second test. This reflects a very good correlation between the remotely-determined values and the true mass data for both experiments (within a constant).

The results of this testing showed strong correlation and good within-test repeatability. However, there are multiple areas in which improvements could be made. First, it is critical that all of the measured signals are synchronized. The most accurate method of achieving this synchronization is by utilizing a single data acquisition system for all measurements (audio and video). Second, the data acquisition system must begin measuring the vehicle at least 2 s prior to any forward motion or acceleration from a constant velocity initial motion state. This will ensure that the zero-torque condition is captured. Third, the grade of the road where the test vehicle is being operated should be measured precisely and accounted for using Equation 14. Finally, observation of the test vehicle should be extended. Increasing the measurement window to 10 to 15 s should improve the overall effectiveness of the system and make the measurements more robust to noise and measurement error. This could be achieved by reducing the frame rate of the video acquisition system, as the 1,200 frames-per-second rate of the Vision Research Phantom v5.1 camera proved to be faster than is required. A more reasonable 100 to 300 frame rate camera should provide more than adequate temporal resolution.

### *Acknowledgments*

The authors would like to thank the United States Department of Energy, National Nuclear Security Administration, Office of Defense Nuclear Nonproliferation (NA-22) for their support of this work under contract number DE-AC09-08SR22470/AC799980. Special thanks are expressed to Dr.

Alfred Garrett, Dr. David Coleman, and Dr. Larry Koffman of the Savannah River National Laboratory for their invaluable assistance in facilitating the field experiments carried out at the Savannah River Site in Aiken, South Carolina.

### *References*

- 1 B. Jacob and V. Feypell-de La Beaumelle, “Improving truck safety: Potential of weigh-in-motion technology,” *IATSS research* **34**(1), 9–15 (2010).
- 2 B. Taylor, A. Bergan, N. Lindgren, and C. B. P. D. P. Eng, “The importance of commercial vehicle weight enforcement in safety and road asset management,” *Annual Review* pp **234**, 237 (2000).
- 3 K. Helmi, T. Taylor, and F. Ansari, “Shear force–based method and application for real-time monitoring of moving vehicle weights on bridges,” *Journal of Intelligent Material Systems and Structures* **26**(5), 505–516 (2015).
- 4 F. Beer, E. Johnston, and J. DeWolf, “Mechanics of materials, 2002,” *McGraw-Hill, New York* (2002).
- 5 J. Walker, D. Halliday, R. Resnick, and J. Walker, *Fundamentals of physics*, Wiley New York (2008).
- 6 R. Gonzalez and R. Woods, *Digital Image Processing*, Pearson/Prentice Hall (2008).



**Troy R. McKay** is a PhD candidate at the Rochester Institute of Technology. He earned his BA in Applied Physics from SUNY Geneseo in 2003. He holds an MS from SUNY Buffalo in Electrical Engineering. He is currently the founder and President of Hyperspectral Solutions, LLC.



**Carl Salvaggio** received his BS and MS degrees in Imaging Science from the Rochester Institute of Technology (RIT) in 1987. He received his PhD in Environmental Resource Engineering in 1994 from the State University of New York, College of Environmental Science and Forestry, at Syracuse University. From 1994 to 2002, he worked on model validation and database development for the defense intelligence community. Since 2002 he has been a professor of Imaging Science at RIT.



**Jason W. Faulring** earned his BS in Computer Engineering from the Rochester Institute of Technology (RIT) in 2003. As a senior systems engineer at RIT's remote sensing laboratory from 2003 to 2015, he developed novel airborne and ground-based sensing systems for the lab's research efforts. He is currently a senior engineer and partner at AppliedLogix, LLC developing custom hardware and software solutions.



**Glenn D. Sweeney** received his BS degree in Imaging Science from the Rochester Institute of Technology in 2013, and his MSc in Color Science from the CIMET University consortium in 2015. After graduation he has entered the workforce designing image quality test equipment for mobile camera systems.